LAWRENCE
LIVERMORE
NATIONAL
LABORATORY

LLNL-TR-416150

# Monte Carlo Simulations of Ultra-High Energy Resolution Gamma Detectors for Nuclear Safeguards

A. Robles, O. B. Drury, S. Friedrich

August 25, 2009

## Disclaimer



This work performed under the auspices of the U.S. Department of Energy by Lawrence Livermore National Laboratory under Contract DE-AC52-07NA27344.

# Monte Carlo Simulations of Ultra-High Energy Resolution Gamma Detectors for Nuclear Safeguards

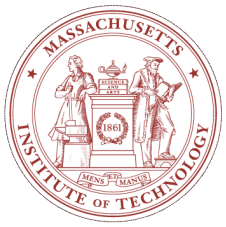


Andrea Robles
Department of Nuclear Engineering, Massachusetts Institute of Technology

Owen B. Drury, Stephan Friedrich
Advanced Detector Group, Lawrence Livermore National Laboratory

Andrea Robles

Owen B. Drury

Stephan Friedrich

Lawrence Livermore National Laboratory
7000 East Avenue, Livermore, CA 94550

August 7, 2009
LLNL-TR-416150

# Abstract

Ultra-high energy resolution superconducting gamma-ray detectors can improve the accuracy of non-destructive analysis for unknown radioactive materials. These detectors offer an order of magnitude improvement in resolution over conventional high purity germanium detectors. The increase in resolution reduces errors from line overlap and allows for the identification of weaker gamma-rays by increasing the magnitude of the peaks above the background. In order to optimize the detector geometry and to understand the spectral response function Geant4, a Monte Carlo simulation package coded in C++, was used to model the detectors. Using a 1 $mm^3$ Sn absorber and a monochromatic gamma source, different absorber geometries were tested. The simulation was expanded to include the Cu block behind the absorber and four layers of shielding required for detector operation at 0.1 K. The energy spectrum was modeled for an Am-241 and a Cs-137 source, including scattering events in the shielding, and the results were compared to experimental data. For both sources the main spectral features such as the photopeak, the Compton continuum, the escape x-rays and the backscatter peak were identified. Finally, the low energy response of a Pu-239 source was modeled to assess the feasibility of Pu-239 detection in spent fuel. This modeling of superconducting detectors can serve as a guide to optimize the configuration in future spectrometer designs.

# Introduction

The safeguarding and accountability of nuclear materials at all points in the fuel cycle depend on our ability to measure the percentage of fissile components in a given material. The uranium fuel that goes into conventional reactors used in the United States, such as pressurized water reactors (PWRs) and boiling water reactors (BWRs), must be enriched to maintain the neutron chain reaction. The fuel is then used up at a certain burn-up rate and eventually taken out of the reactor. When the fuel exits the reactor, it can either be recycled in a reprocessing plant or placed in a storage facility. Proper safeguarding techniques involve tracing the amount of fissile materials in the fuel from the beginning of the cycle to the end. For the case of the spent fuel, the safeguarding relies on the burn-up value declared by the reactor operator. The values are then checked by counting the total gamma-ray activity and/or by measuring the total neutron output. These non-destructive analysis (NDA) tools provide a rough measure of the ratio of fissionable isotopes in a material. Another NDA technique to confirm the burn-up is the use of high-purity germanium detectors (HPGe) to compare the isotopic ratios of certain fission products such as the ratio of Cs-134 (796 keV) to Cs-137 (662 keV), which is proportional to the burn-up (Philips, 1991). The main problem with these techniques is that the emitted gamma-rays from fissile material are obscured by the Compton background originating from the fission products. For example, with the currently used NDA techniques the detection of Pu-239 at low energy is not possible. Very low temperature ultra-high energy resolution gamma-ray detectors such as superconducting cryogenic detectors may make the direct detection of Pu-239 in spent fuel possible.

Superconducting detectors, such as the one pictured in figure 1, offer an order of magnitude improvement in energy resolution over conventional HPGe detectors. The higher resolution leads to higher more discernible peaks. Also, since the actual detectors are quite small (~ 1 $mm^3$), the cross section for higher energy gammas, which cause the low energy Compton background, is small. The improvement of the peak-to-background ratio at lower energies allows for easier detection of weaker gamma-rays. In order to understand and improve these detectors, Monte Carlo simulations are used to model the expected detector response of gamma-rays.

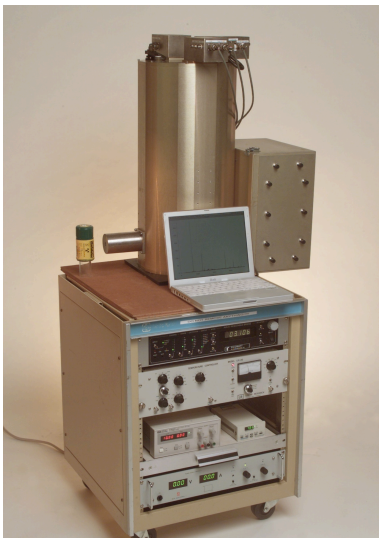

Figure 1: Superconducting gamma spectrometer with readout electronics.

# Background

Cryogenic detectors are composed of a bulk absorber attached to a superconducting thermometer, also known as a transition edge sensor (TES). Both of these are weakly coupled to a cold bath through a thermal conductance (G), as depicted in figure 2. The TES temperature, as seen in figure 3, is held at the transition temperature ($T_c \approx 0.1$ K) between its superconducting and its normal state where the resistance varies sensitively with temperature. The TES measures the temperature change as a change in resistance when a photon deposits energy in the absorber. Since the resistance in the TES is low, a preamplifier known as a superconducting quantum interference device (SQUID) is used to read out the signal.

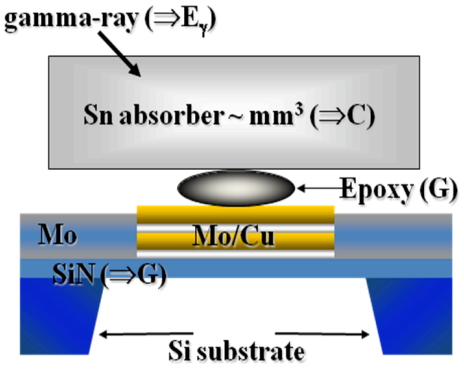


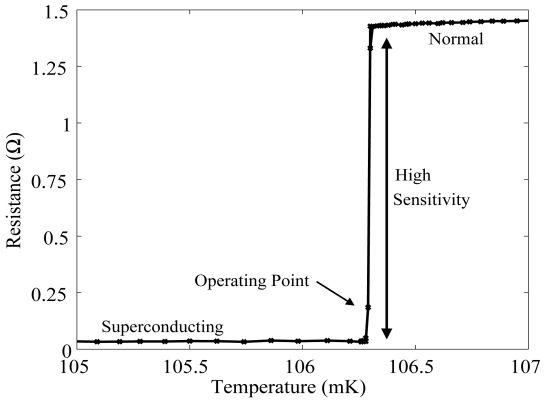


Figure 2 (left): Schematic representation of the detector setup using a Mo/Cu TES and a Sn absorber. Figure 3 (right): The transition between the normal and superconducting state for a Mo/Cu TES absorber.

The energy resolution of superconducting detectors is given by

$$\Delta E_{\mathrm{FWHM}} \approx 2.355\sqrt{k_B T^2 C}, \quad (1)$$

where T is the absolute temperature and C the absorber heat capacity. The absorber size is limited by the requirement that the heat capacity of the material not degrade the energy resolution below a desirable value. For common absorbers made out of Sn or Bi, the volume is limited to ~1 mm$^3$ in order to achieve a resolution below 100 eV (Friedrich et al., 2004). According to equation 1, very low temperatures are necessary in order to achieve a high resolution spectrum. To achieve these low temperatures, the TESs are operated in an adiabatic demagnetization refrigerator (ADR) behind several layers of thermal shielding. An ADR utilizes liquid nitrogen and liquid helium for precooling to 4.2 K, plus two paramagnetic salts to reduce the temperature to ~0.1 K. The cooling cycle begins at 4.2 K by closing the heat switch and inducing a magnetic field, which causes the spins in the salts to align. After the heat of magnetization is carried into the 4.2 K He bath, the heat switch is opened, the magnetic field is turned off and the spins in the salts begin to randomize, thereby taking in energy in the form of heat. The temperature is therefore lowered because the heat is taken from the system. Three layers of shielding help maintain the low temperature. The outer mumetal shield (mostly composed of nickel) is at room temperature (300 K), the 77 K copper shield cooled with nitrogen and the 4.2 K copper shield cooled with helium.

There are different contributions to the response function in superconducting TES gamma detectors. The photopeak occurs when the gamma-ray photon is completely absorbed by the material. In addition to the main peak, there are several other features in the response function that determine the detector's sensitivity. Figure 4 depicts the different sources of the background spectrum that lead to less than the full energy being deposited in the detector. Compton scattering occurs when an incident photon (hν) hits an electron causing the creation of a scattered lower energy photon (hν') and a recoil electron. The energy of the scattered photon depends on the scattering angle (θ) and is given by

$$h\nu' = \frac{h\nu}{1+\left(\frac{h\nu}{m_0 c^2}\right)(1-\cos\theta)}, \quad (2)$$

where $m_0c^2$ (511 keV) is the rest mass energy of the electron (Knoll, 2000). If the scattered photon leaves the material, only part of the energy is deposited in the absorber, hence the origin of the Compton continuum. The Compton continuum is broad because the energy lost ranges from the lowest energy loss ($\theta$=180˚) to the greatest energy loss ($\theta$=0˚). If the photon is not incident on the absorber but instead Compton scatters on the material behind the absorber, a backscatter peak is created. The energy ranges from the lowest energy at $\theta$=180˚ to the greatest possible scatter that still hits the absorber. If the photon Compton scatters in the material in front of the absorber it has a similar effect except that it scatters from the shielding.

Compton scattering also creates a recoil electron that interacts with the material. When an electron is set loose in the absorber, it loses its energy by hitting other electrons, which leads to a cascade of electrons interacting with each other. This only becomes significant from our standpoint when the electron leaves the absorber therefore not all of the energy is deposited leading to extra scattering events.

Some other features of the energy spectrum are the escape and fluorescence peaks. The escape peaks occur when a photon hits the absorber and ejects an electron from the inner atomic shell (usually the K or L shell) leaving an electron hole. The energy needed to eject the electron depends on the specific binding energy associated with the material in that specific orbital. The electron hole leaves the atom unstable and causes an outer orbital electron to fall down to that energy, emitting an x-ray. If this fluorescence x-ray escapes from the absorber, an escape peak occurs in the spectrum, and its energy can be calculated by subtracting the known x-ray energy from the photopeak. Fluorescence peaks are created the same way as escape peaks, except that the incident photon hits the material surrounding the detector instead of the absorber itself. If the emitted x-ray is subsequently captured by the absorber and deposits its energy, it creates a peak in the energy spectrum at the characteristic energy of the x-ray emitted. Another common mechanism of gamma interaction is pair production, which can be neglected here because our sources do not produce lines above 1022 keV.

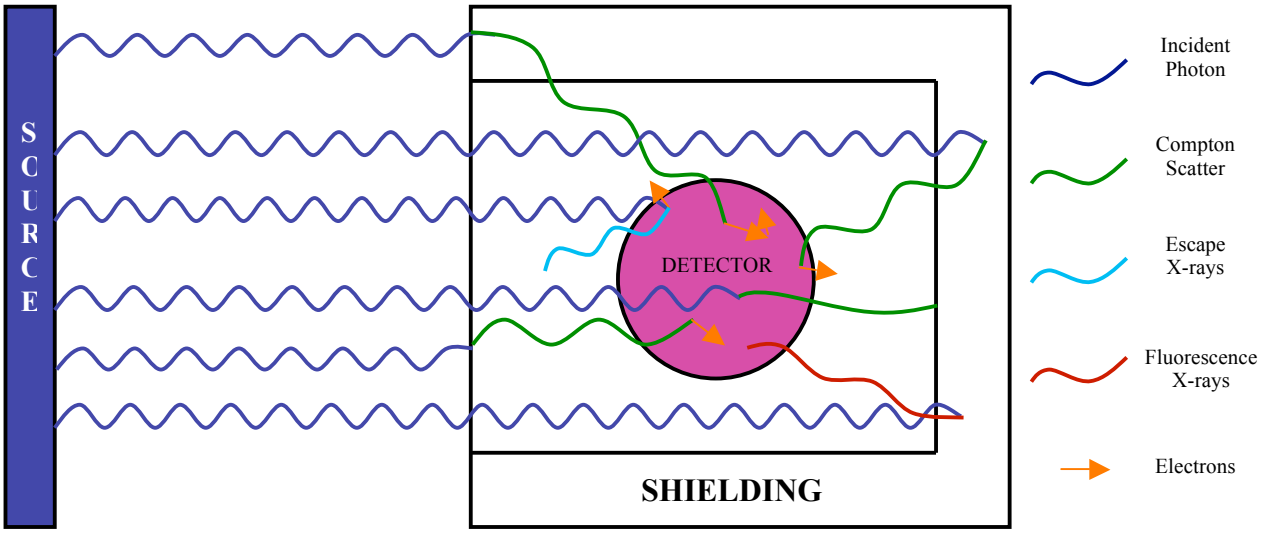


Figure 4: Possible interactions of a gamma source incident on an absorber neglecting pair production.

# Purpose

The modeling of superconducting detectors using Monte Carlo simulations can lead to a better understanding of the factors that influence the detector sensitivity. Through the models, the origins of the features in the spectra can be better understood, and the unnecessary parts that cause an increase in scattering in the response can be minimized or eliminated. The simulation geometry can be altered to understand how to achieve a greater sensitivity in the detector. The models can also be used to predict the response from known sources and to assess the feasibility of certain experiments, for example, the expected spectra from spent fuel.

# Methods

A gamma-ray interacting in matter has a number of different possibilities as to how it deposits its energy, making its energy deposition in a superconducting detector a good candidate for Monte Carlo simulations. Monte Carlo is a class of computational algorithms that rely on the probability of an event to occur to randomly calculate the outcome. Geant4 is a Monte Carlo modeling package coded in C++ used to track the interaction of particles through matter. The user of Geant4 decides on a stepsize, so every time the particle advances one step, the program semi-randomly evaluates what the next move of the particle will be. The decision is semi-random, because it is based off of a physics list that sets the likelihood of different interactions occurring (Agostinelli, 2008). If the simulation is run with 10 events, chances are that only the most common interactions will occur. If the simulation is run with millions of events, then the probability that all interactions will be visible is quite high. Therefore, for favorable results the stepsize should be less than the thickness of the material the particle is going through, and the number of events processed should be large. In our simulations we used a stepsize of 0.01 mm with a minimum of $10^7$ events per configuration.

Geant4 allows the user to add geometries into any configuration and then decide which part will act as the sensitive detector. The energy spectrum is taken in the reference frame of the sensitive detector, and only the energy deposited in the detector is recorded. For example, if a photon misses the detector, hits the background material and scatters back into the detector, the energy lost in the scattering event is not recorded, but the energy deposited in the detector when it scatters back is. In our simulation the sensitive detector is composed of a 1 $mm^3$ piece of tin which serves as the absorber of the TES.

The physics list included in Geant4 allows the user to choose what particle type to use as the incident source. The program also gives the user control as to how the source is going to hit the geometry. The source can be modeled as a point source shooting randomly in all directions, or as a linear source shooting in a random x-y direction. In our simulations the particle gun is a point source shooting in the forward and the backward direction with an angle span of ±32.74°. This is done because the source is encapsulated in a steel cylinder with a small tunnel for the gamma-rays to be guided out. If the source was modeled as a true point source, too much of the events stayed within the cylinder and never reached the detector, leading to a poor spectrum at a high computational cost. Therefore the gun was restricted to include just the scattered photons from the steel container that actually reached the detector. The complete simulation model is depicted in figure 5.

## Results

Initially the model consisted of a bare tin absorber and a particle gun emitting 60 keV (Am-241) and 660 keV (Cs-137) gamma-rays. The dimensions of the tin absorber were changed while maintaining a volume of 1 $mm^3$. From these simulations a typical energy spectrum is observed with the characteristic photopeak, the Compton scattering and the tin escape x-rays, as labeled in figure 6 and figure 7. The most intense and therefore visible escape peaks for tin are due to the $K_{\alpha 1}$ (25.271 keV), the $K_{\alpha 2}$ (25.044 keV) and the $K_{\beta}$ (28.486 keV) escape. The less intense L escape peaks are also visible. The L x-rays have lower energies, which range from 3.443 to 3.904 keV. These simulations do not accurately model the detector because they neglect scattering in the shielding of the detector. However, they do provide an insight as to the best detector geometry. Figure 6 depicts the energy histogram of a 660 keV source of Cs-137 for two different geometries. The spectra are quite similar except for the slightly higher photopeak and lower Compton scatter for the 0.5×1.41×1.41mm case. This occurs because the absorption length at 660 keV is longer, and a thicker absorber will allow more photons to be absorbed, leading to a higher photopeak. A higher photopeak is favorable when identifying unknown sources. In figure 7, a 60 keV source of Am-241 is used and the thinnest absorber has the highest photopeak. This occurs because the absorption length at 60 keV is smaller than the 0.1 mm thickness, and there is more surface area for interaction because the volume stays the same. Therefore, the thinner the absorber at the same volume, the greater the photopeak, as long as the thickness is greater than the absorption length.

For the next set of simulations, as seen in figure 5, we set the tin absorber size to 0.25×2.0×2.0 mm, as appropriate for our TES detector, added a copper heat sink block behind the absorber, and surrounded the absorber with four layers of shielding associated with the different temperature stages. The outer layer is made out of mumetal (mostly nickel), and the three inner layers are copper cylinders with a 0.025 mm thick aluminum window. The source was placed a few centimeters away from the outer layer and encapsulated in an iron cylinder. With this new configuration, new features were visible in the spectrum that more closely match the experimental data. As seen in figure 8, the copper fluorescence is observed at 8 keV and the backscatter peak is visible at around 50 keV for the experimental data. In the case of the

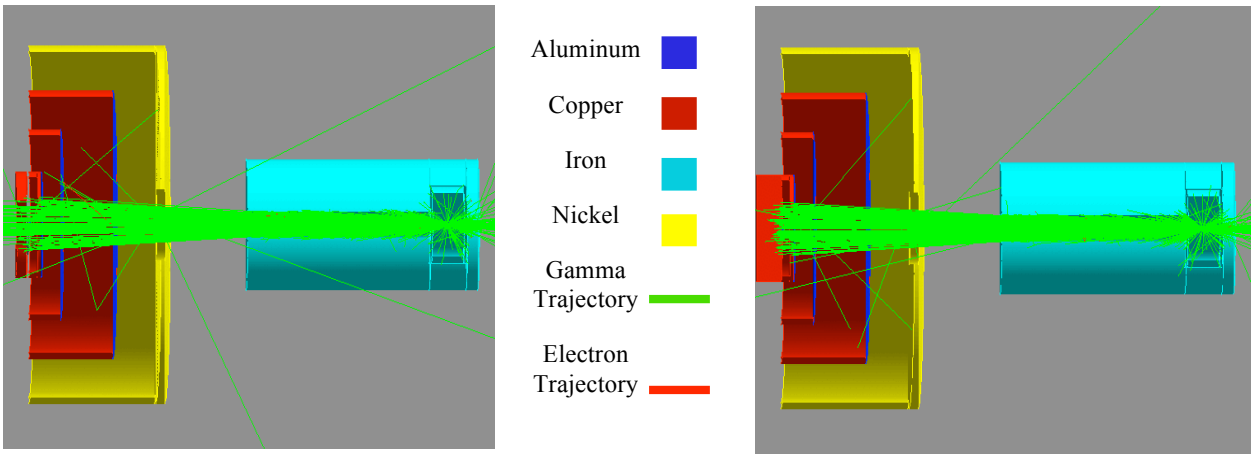


Figure 5: The simulation configuration for a 60 keV gamma source incident on a tin absorber with a copper back (right) and three layers of shielding. The diagram to the left replaces the copper block with a copper ring.

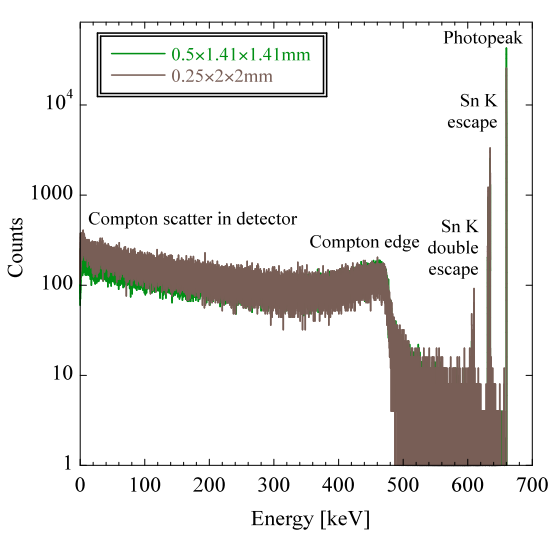


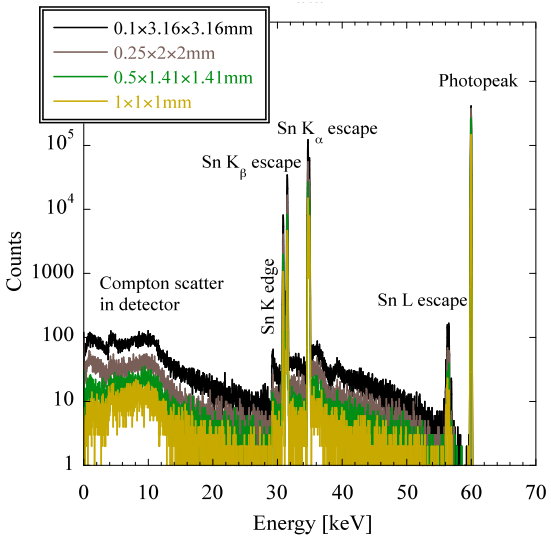


Figure 6 (left): Simulations of a 660 keV gamma source incident on a 1 mm$^3$ tin absorber of different dimensions. Figure 7 (right): The same simulation but using a 60 keV source.

simulation, the scattering peaks due to the shielding are dominant between 40 and 60 keV. Similar to the experimental data, the backscatter peak occurs around 50 keV. However there is a magnitude difference between the two spectra. This difference is probably due to the approximate geometry of the detector in our simulations.

Figure 9 compares the data taken for a Cs-137 source with the simulations. The spectrum matches closely with the magnitude of the Compton scattering. However the backscatter peak is more pronounced in the simulation data. Again, this is likely due to the approximate geometry we used in our simulations. The simulation needs to be further expanded and detailed to more closely match the detector configuration. An interesting peak in this spectrum are the barium x-

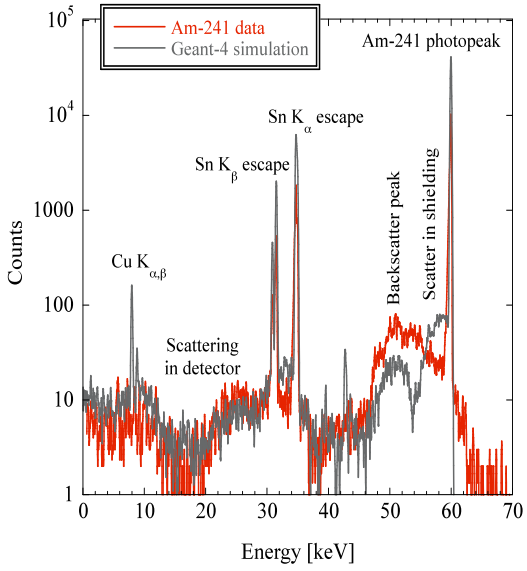


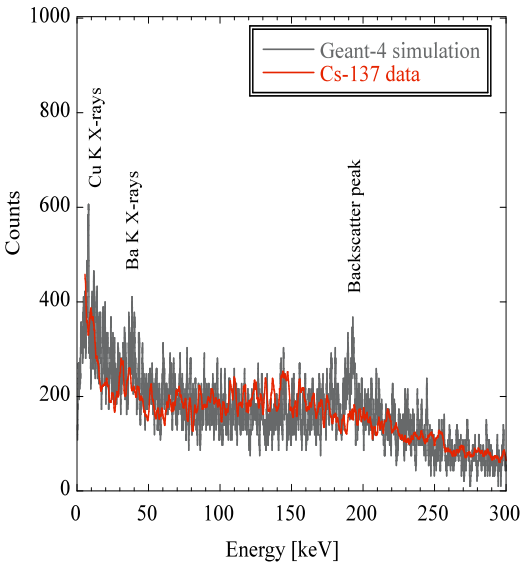


Figure 8 (left): Comparison of the simulation including the copper back and the aluminum/nickel shielding to the experimental data for a 60 keV (Am-241) source. Figure 9 (right): Comparison of the simulation to the ~300 keV dynamic range of the experimental data for a 660 keV (Cs-137) source.

rays at ~40 keV, which arise from the beta decay of Cs-137, since the decay of Cs-137 can remove a K-shell electron from the Ba-137 daughter nucleus. The graph does not extend beyond 300 keV because the TES leaves the linear region of the superconducting transition, and the experimental data are no longer meaningful.

Using the above geometry and a 60 keV source, the simulation was altered by replacing the copper block with a copper ring (figure 5). Changing the geometry minimizes some of the escape peaks due to copper, as seen in figure 10. Another interesting change is in the region between 40 and 50 keV. The copper ring spectrum reduces the backscattering from the copper into the tin absorber where it deposits the remainder of its energy. One of the strengths of the simulation is that the sources of the spectral features can be accurately identified, and could then be eliminated. Another interesting note is how small changes can cause important changes in the spectrum. In order to improve the detectors, all of the parts have to be modeled properly.

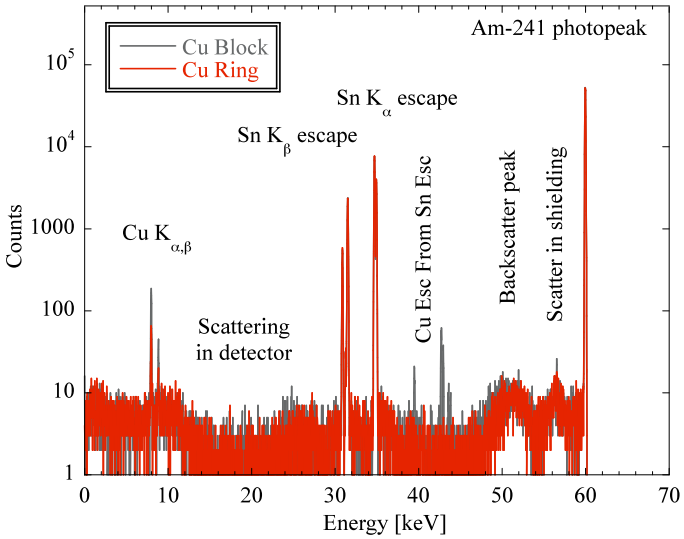


Figure 10: Comparison of the energy spectra for a 60 keV gamma source when the back copper block is substituted for a copper ring.

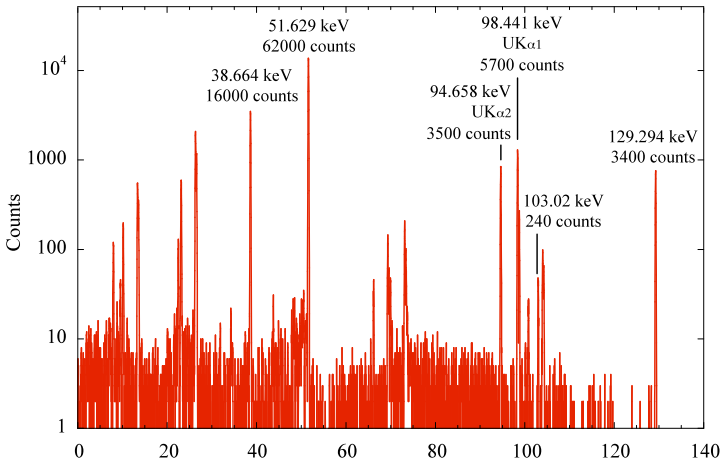


Figure 11: Simulation of the six strongest Pu-239 emission lines that lie within the dynamic range of the TES. The other visible peaks are x-ray escape peaks.

In order to examine the applications of our superconducting detectors the low energy response of Pu-239 was modeled (figure 11). The six strongest lower energy emissions peaks are clearly visible above the scattering in the detector. The hope is that the high resolution of these detectors will allow the emission peaks of isotopes like Pu-239 to also be discernible from the background in a spent fuel source. For example, the ratio of Pu-239 to Cs-137 varies from 10:1 to 1:1 depending on the burn-up at the end of the fuel cycle. However, since the gamma emissions of Cs-137 are ~6 orders of magnitude higher than those of Pu-239, the Pu-239 lines are masked by the Compton background from the fission products. Superconducting detectors can minimize the Compton background because of the small cross section for higher energy gammas. Therefore these detectors are good candidates for identifying spent fuel if the necessary number of counts can be

collected. In the future we will simulate the expected response from the fission products to determine the peak-to-Compton ratio at low energies for realistic spent fuel compositions.

## Conclusion

Ultra-high energy resolution superconducting TES gamma-ray detectors exploit the steep change in resistance when a superconductor moves from its normal to its superconducting state at very low temperatures. Small (~ 1 $mm^3$) superconducting detectors operating at 0.1 K can have an energy resolution below 100 eV FWHM, an order of magnitude better than HPGe detectors. The increase in resolution reduces line overlap and allows for the identification of weaker gamma-rays at lower energies by increasing the magnitude of the peaks and decreasing the scattering background. Using the Geant4 Monte Carlo simulation package, the detectors were modeled and the spectral features were identified. Using a simple bare absorber and a monochromatic gamma source it was deduced that for a higher photopeak a thinner absorber with greater surface area is beneficial, as long as the thickness is less than the absorption length. The comparison between the simulations and the experimental data showed that the spectra matched well except for a few errors where the magnitude of the scattering background was different. The simulations can be further improved to more closely match the configuration of the detectors.

The simulations can be used to predict the gamma spectra of known sources. For example, we can simulate the response of the TES detector to radiation from nuclear spent fuel to assess if it is possible to directly detect the emission from Pu-239 on top of the Compton background from the fission products. The Geant4 simulations were adapted to model the low energy response of Pu-239. Future work will focus on simulating the response to typical fission products to determine under which condition the Pu emissions are still visible in their presence. The simulations can lead to further improvement in the resolution by adjusting the detector geometry and the cryostat configuration.

## Acknowledgements

This work was funded by the U.S. Department of Energy, Advanced Fuel Cycle Initiative under grant LL0915040309. Andrea Robles gratefully acknowledges the support of the NNSA Consortium Internship Program and of the Society of Professional Hispanic Engineers (SHPE). This work was performed under the auspices of the U.S. Department of Energy by Lawrence Livermore National Laboratory under contract DE-AC52-07NA27344.

## References

Agostinelli, S., et al. (Geant4 collaboration), (2008). *Geant4 User's Guided for Application Developers, Version: geant4 9.2*. Retrieved June 1st, 2009, from http://geant4.web.cern.ch/geant4/UserDocumentation/UsersGuides/ForApplicationDeveloper/html/

Friedrich, S., Terracol, S.F., Miyazaki, T., Drury, O.B., Ali, Z.A., Cunningham, M.F., et al., & Burger, A., James, R., Franks, L. (Eds.). (2004). Proceedings from SPIE Vol. 5540: *Design of a*

*Multi-Channel Ultra-High Resolution Superconducting Gamma-Ray Spectrometer*. Bellingham, WA: SPIE.

Knoll, G.F., (2000). *Radiation Detection and Measurement* (3rd ed.). New York: John Wiley & Sons, Inc.

Phillips, J.R. (1991). *Passive Nondestructive Assay of Nuclear Materials* (Reilly, D., Ensslin, N., Smith, H., Kreiner, S., Eds.). Los Alamos, NM: NUREG.